Article

Convergence of Dissipation and Impedance Analysis of Quartz Crystal Microbalance Studies

Yaozhong Zhang, Binyang Du, Xinan Chen, and Hongwei Ma

Anal. Chem., **2009**, 81 (2), 642-648 • DOI: 10.1021/ac8019762 • Publication Date (Web): 11 December 2008

Anal. Chem. **2009,** *81,* 642–648

Convergence of Dissipation and Impedance Analysis of Quartz Crystal Microbalance Studies

Yaozhong Zhang,[†] Binyang Du,*[,‡] Xinan Chen,[†] and Hongwei Ma*[,†,§]

Key Laboratory of Macromolecular Synthesis and Functionalization (Ministry of Education), Department of Polymer Science & Engineering, Zhejiang University, Hangzhou 310027, and Department of Biomedical Engineering, College of Engineering, Peking University, Beijing 100871, China

A quartz crystal microbalance (QCM) consists of a resonator, which measures the resonance frequency of the quartz slab. When coupled with a network analyzer or coupled with impulse excitation technology, QCM gives additional impedance or dissipation information, respectively. This report provides a set of equations that bring the QCM community a convergence of the dissipation and impedance analysis. Equations derived from the complex frequency shift were applied to quantitatively analyze the dissipation data of polymer brushes obtained from QCM-D. The obtained viscoelastic properties of polymer brushes were then compared with those obtained by the Voigt model method. We believe that these equations will be useful in quantitative studies of interfacial phenomena accompanied with mass or viscoelasticity changes.

Three types of quartz crystal microbalance (QCM) are currently in use: (i) the simplest version measures the resonance frequency (f), or sometime the resistance (R) of a quartz crystal by an oscillator,[1] which is an essential component for all three types of QCM, (ii) a resonator coupled with a network analyzer for impedance measurement, and (iii) an oscillator coupled with impulse excitation technology for dissipation measurement. The introduction of Sauerbrey equation in 1959, which revealed a simple linear relation between the deposited mass (Δm_f) and the corresponding frequency shift (Δf), has made QCM a popular online monitor for vacuum deposition:[2,3]

$$\frac{\Delta f_n}{f_0} = \frac{-2f_n}{Z_q}\Delta m_f = \frac{-2f_n}{Z_q}\rho_f d_f \qquad (1)$$

where Δf_n and f_n are the frequency shift and the resonance frequency at overtone number n, respectively, and $f_n = nf_0$, $n = 1, 3, 5, 7, 9, 11, 13...$, Δm_f is the areal mass density, ρ_f and d_f are the density and thickness of the deposited film, respectively, and $Z_q = 8.8 \times 10^6$ kg m^{-2} s^{-1} is the acoustic impedance of the crystalline quartz.

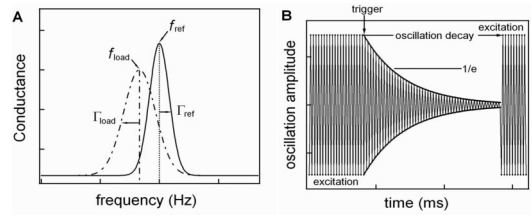

Figure 1. Typical experimental signals from (A) impedance analysis, where $\Delta f = f_{load} - f_{ref}$ and $\Delta\Gamma = \Gamma_{load} - \Gamma_{ref}$, and (B) the impulse excitation setup.

The deduction of the Sauerbrey equation is based on the assumption that the deposited mass can be treated as quartz itself (i.e., the deposited mass is equal to the increase of quartz thickness). More rigorous physical analysis also leads to a similar conclusion for most materials (metals and polymers) under vacuum conditions.[3] However, this linear relation fails for soft thin films, especially for viscoelastic polymer in good solvents. While this was viewed as an obstacle for the development of QCM toward biosensor applications, researchers later realized that the viscoelastic properties and other useful physical information of the soft thin films could be extracted out from the measured impedance or dissipation data.

A network analyzer was introduced to provide a complete impedance spectrum of the quartz crystal (Figure 1A), which contains the information of resonance frequency and half-bandhalf-width.[4] QCM systems based on impedance analysis are, for instance, available from Resonant Probes or KSV Instruments. Typically, one infers frequency and bandwidth from the impedance spectra. Various groups have described the frequency and bandwidth and related these to the viscoelastic properties of the sample.[5−9] Johannsmann, in particular, has emphasized how information on the viscoelastic properties of the adsorbed film can be deduced from such data.[10−14]

* To whom correspondence should be addressed. E-mail: duby@zju.edu.cn (B.D.); hwma2008@sinano.ac.cn (H.M.).

† Peking University.

‡ Zhejiang University.

§ Current address: Suzhou Institute of Nano-Tech and Nano-Bionics, Chinese Academy of Sciences, Suzhou 215125, P. R. China.

(1) http://www.thinksrs.com/products/QCM100.htm.
(2) Sauerbrey, G. *Z. Phys.* **1959**, *155*, 206–222.
(3) Lu, C., Czanderna, A. W., Eds. *Methods and Phenomena-Their Applications in Science and Technology*; Elsevier: New York, 1984; p 393.
(4) Buttry, D. A.; Ward, M. D. *Chem. Rev.* **1992**, *92*, 1355–1379.
(5) Eggers, F.; Funck, Th. *J. Phys. E: Sci. Instrum.* **1987**, *20*, 523–530.
(6) Nakamoto, T.; Moriizumi, T. *Jpn. J. Appl. Phys* **1990**, *29*, 963–969.
(7) Bandey, H. L.; Martin, S. J.; Cernosek, R. W.; Hillman, A. R. *Anal. Chem.* **1999**, *71*, 2205–2214.
(8) Lucklum, R.; Behling, C.; Hauptmann, P. *Anal. Chem.* **1999**, *71*, 2488–2496.
(9) Benes, E. *J. Appl. Phys.* **1984**, *56*, 608.
(10) Johannsmann, D.; Mathauer, K.; Wegner, G.; Knoll, W. *Phys. Rev. B* **1992**, *46*, 7808–7815.
(11) Domack, A.; Prucker, O.; Ruhe, J.; Johannsmann, D. *Phys. Rev. E* **1997**, *56*, 680–689.
(12) Etchenique, R.; Weisz, A. D. *J. Appl. Phys.* **1999**, *86*, 1994–2000.

10.1021/ac8019762 CCC: $40.75
Published on Web 12/11/2008

Especially, the high frequency shear compliance of the thin film in liquid can be obtained from the ratio ($\Delta\Gamma/\Delta f$) of the bandwidth shift ($\Delta\Gamma$) and the frequency shift (Δf) by referencing to the bare quartz crystal in liquid. Although no thickness measurement is required, one has to make guesses on the density of the deposited film. Martin and Hillman groups investigated the shear modulus and film resonance phenomena of thin films on quartz crystal by analyzing the impedance and admittance from the equivalent circuit of the QCM.[7,15–18]

In early 1950s, impulse excitation has been used on torsional resonators.[19] In 1995, Rhodal et al. applied the impulse excitation method to measure the dissipation of oscillation (Figure 1B).[20] Impulse excitation means to periodically switch on and off the driving power to the quartz crystal at the resonance frequency and to record the free decay of the oscillation. By fitting the free decay of oscillation with eq 2, one can obtain the resonance frequency and acoustic energy dissipation (D) of the quartz crystal. The energy dissipation is a dimensionless quantity given by eq 3:

$$A(t) = A_0\, e^{-t/\tau} \sin(2\pi f t + \phi) \tag{2}$$

$$D = \frac{1}{\pi f \tau} = \frac{1}{Q} = \frac{E_{\text{dissipated}}}{2\pi E_{\text{stored}}} \tag{3}$$

where Q is the quality factor, E_{stored} is the energy stored in the oscillating system, and $E_{\text{dissipated}}$ is the energy dissipated during one period of oscillation.

Since the dissipation can be directly measured by the impulse excitation technique, the QCM device using the impulse excitation technique is usually called quartz crystal microbalance with dissipation monitoring (QCM-D). Currently, such an instrument is commercially available from Q-Sense (Q-Sense, Gothenburg, Sweden). While impulse excitation is a general term, "QCM-D" is a trademark by q-sense and denotes this particular instrument. While Johanssmann et al. applied the equivalent circuit approach to realize the quantitative impedance analysis, Kasemo et al. started from a continuous mechanics model, i.e., the Voigt model (or the acoustic multilayer formalism), to correlate the measured parameters (frequency shift Δf and dissipation shift ΔD) with the viscoelasticity of the thin film.[11,21] The "Voigt model" is used to describe the situations, where the storage modulus, η, and the viscosity, μ, are independent of frequency. If η and μ are allowed to depend on frequency, the "Voigt model" is equivalent to the acoustic multilayer models. Note that the viscoelastic parameters of polymeric materials usually depend on frequency in most cases.

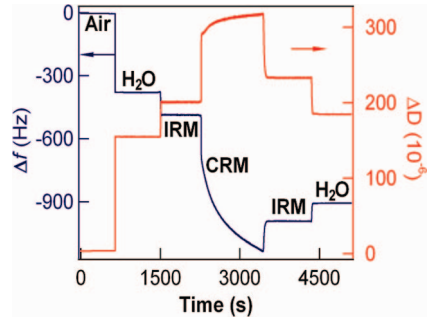

Figure 2. Typical time evolution of frequency (in blue) and dissipation (in red) changes for in situ SI-ATRP of OEGMA526. The final poly(OEGMA526) brush had a dry film thickness of 33 nm.

Similar to the impedance method, in the Voigt model either the density or the thickness of the thin film has to be measured independently.[22–25] Thus, the accurate determination of the density or thickness of the deposited film in the wet environment becomes a necessary yet formidable challenge.

Most recently, Ma et al. combined QCM-D and elllipsometry to investigate the physical properties of polymer brushes prepared from surface initiated atom transfer radical polymerization (SI-ATRP or SIP).[26,27] The application of SI-ATRP provided a unique opportunity in that SI-ATRP enabled the control of film thickness in steps of nanometers (that was to increase deposited mass in very small steps). Starting from the Voigt model, they deduced a set of analytical equations to quantitatively interpret the frequency and dissipation data, including the viscosity (η), elasticity (μ), and density ($\rho_{\text{f,dry}}$ and $\rho_{\text{f,wet}}$) of the polymer brushes.

It is clear that both impedance and dissipation are valid probes for the viscoelasticity of the deposited films.[28,29] In fact, D and Γ are connected by eq 4:

$$D = Q^{-1} = \frac{2\Gamma}{f} \tag{4}$$

where Q is the quality factor. However, no efforts, to the best of our knowledge, were found to compare the results obtained by these two approaches. This report tends to bring the QCM community a convergence of the dissipation and impedance analysis. Starting from eq 4, we will first apply the equations of complex frequency shift derived by Johannsmann et al. to quantitatively analyze the QCM-D data of polymer brushes. The obtained viscoelastic properties of polymer brushes will then be compared with those by the Voigt model. The "Voigt-based modeling" is typically carried out by means of a software package called "Q-tools" from q-sense. The acoustic multilayer formalism is implemented in a software package called QTM, which is available for download at http://home.tu-clausthal.de/~pcdj/QCM_Modeling_QTM.zip.

(13) Johannsmann, D. *J. Appl. Phys.* **2001**, *89*, 6356–6364.
(14) Du, B. Y.; Johannsmann, D. *Langmuir* **2004**, *20*, 2809–2812.
(15) Lucklum, R.; Behling, C.; Cernosek, R. W.; Martin, S. J. *J. Phys. D: Appl. Phys.* **1997**, *30*, 346–356.
(16) Martin, S. J.; Bandey, H. L.; Cernosek, R. W.; Hillman, A. R.; Brown, M. J. *Anal. Chem.* **2000**, *72*, 141–149.
(17) Hillman, A. R.; Jackson, A.; Martin, S. J. *Anal. Chem.* **2001**, *73*, 540–549.
(18) Hillman, A. R. The Electrochemical Quartz Crystal Microbalance. In *Encyclopedia of Electrochemistry*, Vol. 3; Bard, A. J., Stratmann, M., Eds.; Wiley-VCH Verlag GmbH & Co. KGaA: Weinheim, Germany, 2003; pp 230–289.
(19) Sittel, K.; Rouse, P. E.; Bailey, E. D. *J. Appl. Phys.* **1954**, *25*, 1312.
(20) Rodahl, M.; Hook, F.; Krozer, A.; Brzezinski, P.; Kasemo, B. *Rev. Sci. Instrum.* **1995**, *66*, 3924–3930.
(21) Voinova, M. V.; Rodahl, M.; Jonson, M.; Kasemo, B. *Phys. Scr.* **1999**, *59*, 391–396.
(22) Munro, J. C.; Frank, C. W. *Macromolecules* **2004**, *37*, 925–938.
(23) Muller, M. T.; Yan, X. P.; Lee, S. W.; Perry, S. S.; Spencer, N. D. *Macromolecules* **2005**, *38*, 3861–3866.
(24) Brass, D. A.; Shull, K. R. *Langmuir* **2006**, *22*, 9225–9233.
(25) Dutta, A. K.; Belfort, G. *Langmuir* **2007**, *23*, 3088–3094.
(26) He, J.; Wu, Y. Z.; Wu, J.; Mao, X.; Fu, L.; Qian, T. C.; Fang, J.; Xiong, C. Y.; Xie, J. L.; Ma, H. W. *Macromolecules* **2007**, *40*, 3090–3096.
(27) Fu, L.; Chen, X. A.; He, J. A.; Xiong, C. Y.; Ma, H. W. *Langmuir* **2008**, *24*, 6100–6106.
(28) Kanazawa, K. K. *J. Electroanal. Chem.* **2002**, *524*, 103–109.
(29) Johannsmann, D. *Phys. Chem. Chem. Phys.* **2008**, *10*, 4516–4534.

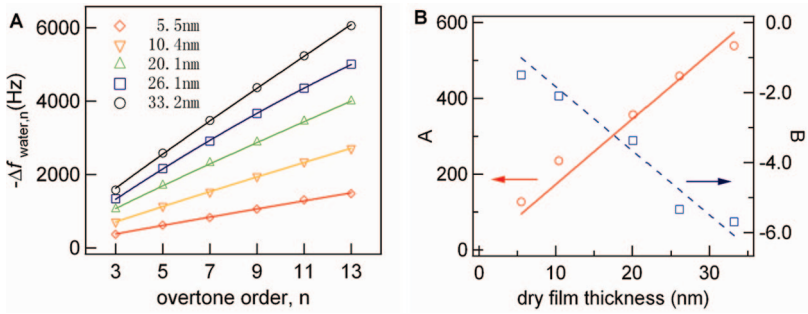

Figure 3. The frequency change dependence on overtone number *n*. (A) The value of Δf_{water} was plotted against *n* for different dry film thickness and fitted according to eq 8. The overtone numbers (*n*) are 3, 5, 7, 9, 11, and 13; (B) fitted values of *A* and *B* show simple linear relations with dry film thickness (force to pass the original point), which was in agreement with eqs 9 and 10. The slope k_A was 17.28 ($R^2 \sim 0.99$) and k_B was −0.18 ($R^2 \sim 0.94$).

Scheme 1. Polymer Brushes Were Deposited onto Quartz by Conducting in Situ SIP in QCM-D[a]

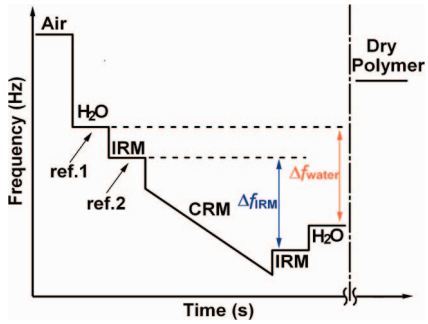

[a] Thus, the value of Δf was read directly from the $f-t$ curve, see Figure 2 for ΔD and $D-t$ curve.

Table 1. List of *k* Values, Calculated $\rho_{f,wet}$, and J_f'' for Poly(OEGMA) Brushes in Liquid

monomer	initiator density	k_A	k_B	$\rho_{f,wet}$ (kg m^{-3})	J_f'' (MPa^{-1})
526 in water	1.00	17.28	−0.18	1521	0.57
526 in IRM	1.00	16.50	−0.20	1452	0.64
475 in water	1.00	20.17	−0.35	1775	1.10
475 in water	0.42	21.54	−0.29	1896	0.93
475 in water	0.15	20.17	−0.33	1775	1.02

EXPERIMENTAL SECTION

The initiator thiol (ω-mercaptoundecyl bromoisobutyrate) and QCM chips were received from HZDW (Hangzhou, China) as gifts. QCM chips with biotin functionalized matrix were obtained from HRBio (Beijing, China). Oligo(ethylene glycol) methacrylate, $M_n = 475$ (OEGMA475) and 526 (OEGMA526) were purchased from Aldrich.

SIP in QCM-D. The initiator thiol modified QCM chip was placed in a Q-Sense E4 sensor (Q-Sense, Gothenburg, Sweden). The activator generated by electron transfer (AGET) SIP was applied to grow polymer brushes.[26] Incomplete reaction mixture (IRM) was prepared by mixing deoxygenated MilliQ-water and methanol in a 1/1 ratio. Complete reaction mixture (CRM) was prepared by the mixing well of two parts. Part 1 was prepared by adding a specified amount of $CuCl_2$/Bipy (1/2 mol ratio) and a fixed amount of monomer to 5 mL of IRM. Part 2 was prepared by adding a specified amount of ascorbic acid (AscA) to 5 mL of IRM. Two parts were mixed together in a glovebox resulting in CRM, which had a mole ratio of monomer/$CuCl_2$/Bipy/AscA = 200/0.7/1.4/0.7, with a feed [$CuCl_2$] of ~2 mM.

The QCM-D was first primed with water and IRM until stable baselines were established. Polymerization was initiated by pumping CRM to the sensor cell at a speed of 70 mL h^{-1} (1~2 min) and reduced to ~3 mL h^{-1} after complete exchange of IRM with CRM (indicated by color change, from colorless to red). SIP was continued for a specified time (30−600 min) at ~25 °C and monitored by QCM-D in real time. The QCM-D instrument has an integrated temperature control component, which ensured the sensor chamber was in a thermostat environment. The polymerization was stopped by replacing CRM with IRM and rinsed with IRM until a stable baseline was reached. Samples were finally pulled out of the sensor cell and rinsed with methanol and MilliQ-water and dried under flowing nitrogen before ellipsometry measurement.

Ellipsometry. Film thickness was measured on an M-2000V spectroscopic ellipsometer (J. A. Woollam Co., Inc.) at angles of 65°, 70°, and 75° and wavelengths from 500 to 800 nm. Ellipsometric data were fitted for the thickness with material specific models, i.e., SAMs and poly(OEGMA) films with fixed (*An*, *Bn*) values of (1.45, 0.01) and (1.46, 0.01), respectively, using a Cauchy layer model. The ellipsometric thickness for each sample was independently measured at six different locations and is reported as the average ± standard error. For wet thickness, the measurement was conducted in a liquid cell at an angle of 70° and wavelengths from 500 to 800 nm and fitted for both thickness and optical properties.

RESULTS AND DISCUSSION

Equations. For any external loading on the quartz crystal, the complex frequency shift (Δf_n^*) is given as eq 5:[13]

$$\frac{\Delta f_n^*}{f_0} = \frac{\Delta f_n + i\Delta\Gamma_n}{f_0} \cong \frac{iZ_{load,n}}{\pi Z_q} \tag{5}$$

where $Z_{load,n}$ is the acoustic impedance of the load at overtone number *n*, f_0 is the fundamental resonance frequency of the quartz crystal (i.e., $n = 1$), Δf_n is the frequency shift at overtone number *n*, and $\Delta\Gamma_n$ is the half-band-half-width shift.

For a viscoelastic thin film in a liquid, $Z_{load,n}$ is given by eq 6:[13]

$$Z_{load,n} \approx Z_{liq,n} + i2\pi n f_0 \rho_f d_f \left(1 - \frac{Z_{liq,n}^2}{Z_{f,n}^2}\right) \tag{6}$$

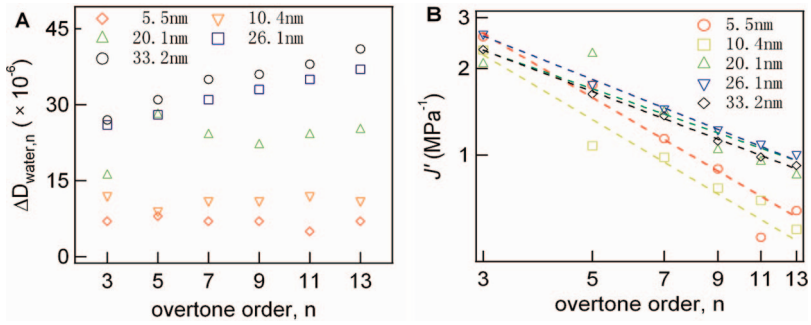

Figure 4. (A) The dissipation change dependence on overtone number n. The value of $\Delta D_{water,n}$ was plotted against n for different $t_{f,dry}$. (B) The value of J_f' was calculated according eq 14 and was plotted against n for different $t_{f,dry}$ in log−log scale and fitted linearly (dashed lines). The R^2 values for all fits were >0.94.

Table 2. Shear Compliance of Poly(OEGMA526) Brushes with Various Thickness in Water and IRM, Respectively, Calculated from Equation 14

thickness (nm)	J_f' (MPa^{-1}, water)	J_f' (MPa^{-1}, IRM)
5.5	$9.05n^{-1.08}$	$9.18n^{-1.09}$
10.4	$5.53n^{-0.90}$	$5.53n^{-0.88}$
20.1	$5.32n^{-0.70}$	$5.29n^{-0.69}$
26.1	$5.22n^{-0.65}$	$5.14n^{-0.64}$
33.2	$4.66n^{-0.64}$	$4.57n^{-0.63}$

where $Z_{f,n} = (\rho_f G_f)^{0.5} = (\rho_f/J_f)^{0.5}$ ($G_f = G'_f + iG_f''$ is the shear modulus, and $J_f = G_f^{-1} = J'_f - iJ_f''$ is the compliance) and $Z_{liq,n} = (i\omega\rho_{liq}\eta_{liq})^{0.5}$ is the acoustic impedance of the film and the liquid, and ρ_f and d_f are the wet film density and thickness in liquid, respectively.

When the frequency and half-band-half-width of bare quartz crystal in liquid are taken as reference states, one has eq 7:

$$\frac{\Delta f_n^*}{f_0} = \frac{\Delta f_n + i\Delta\Gamma_n}{f_0} \approx \frac{-2nf_0 d_f \rho_f}{Z_q}\left(1 + \frac{2\pi n f_0 \rho_{liq}\eta_{liq}}{\rho_f} J_f'' - \frac{i2\pi n f_0 \rho_{liq}\eta_{liq}}{\rho_f} J_f'\right) \quad (7)$$

From eq 7, one has eq 8:

$$-\Delta f_n = \frac{2f_0^2 d_f}{Z_q}(\rho_f n - 2\pi f_0 \rho_{liq}\eta_{liq} J_f'' n^2) = An + Bn^2 \quad (8)$$

where the values of A and B are defined by eqs 9 and 10, and both are assumed to be independent of the overtone number n.

$$A = \frac{2f_0^2 \rho_f d_f}{Z_q} \quad (9)$$

$$B = \frac{-4\pi f_0^3 \rho_{liq}\eta_{liq} d_f J_f''}{Z_q} \quad (10)$$

$$\Delta\Gamma_n = \frac{4\pi f_0^3 \rho_{liq}\eta_{liq} d_f J_f' n^2}{Z_q} \quad (11)$$

If the wet film thickness d_f was known or measured independently, the density ρ_f, elastic compliance J_f'' and J_f' of the thin film can be calculated from eqs 8 and 11, respectively.

Considering the relation of D and Γ, the above eqs 8 and 11 can be also applied to analyze the experimental data obtained by the QCM-D technique. From eq 4, we have eq 12 for the calculation of the shift of half-band-half-width:

$$\Delta\Gamma_n = \Gamma_{FiL,n} - \Gamma_{liq,n} \approx \frac{nf_0(D_{FiL,n} - D_{liq,n})}{2} \quad (12)$$

where $D_{liq,n}$ and $D_{FiL,n}$ are the dissipation changes of bare quartz in liquid and quartz coated with a thin film in the same liquid (the subscript FiL), respectively; $\Gamma_{liq,n}$ and $\Gamma_{FiL,n}$ are the corresponding half-band-half-width for quartz in liquid and polymer coated quartz in the same liquid, respectively.

Inserting eq 12 into eq 11, one has eq 13:

$$\Delta D_n = D_{FiL,n} - D_{liq,n} = \frac{1}{Z_q} 8\pi f_0^2 \rho_{liq}\eta_{liq} d_f J_f' n \quad (13)$$

where ΔD_n is the dissipation shift of quartz coated with thin film in liquid referencing the bare quartz in liquid. Alternately, J_f' can be also calculated from the ratio of $-\Delta D/\Delta f$.[14] By insertion of eq 13 into eq 8 and approximating under condition $An \gg -Bn^2$ (see Figure 3B for details), we have eq 14:

$$-\frac{\Delta D_n}{\Delta f_n} \cong \frac{4\pi\rho_{liq}\eta_{liq} J_f'}{\rho_f} \quad (14)$$

Equation 12 is the essential result, which serves to bring the dissipation and impedance analysis together. Equations 8, 13, and 14 can be directly applied to analyze the experimental data of the QCM-D technique. For example, the plot of ΔD against Δf was used in many papers as an indication of physical state change.[30−38]

Poly(OEGMA526). Monomer OEGMA526 was tested because of its demonstrated biomedical applications.[39] Poly(OEGMA526) was deposited onto quartz by in situ SIP, thus the value of Δf and ΔD were read directly from $f-t$ and $D-t$ curves (Scheme 1 and Figure 2). The experiment was conducted as previously reported.[26,27] Briefly, an initiator functionalized QCM chip was loaded to the sensor chamber of an E4 QCM-D instrument, oscillated in air to measure its absolute frequency, which was automatically set to zero. Water was then pumped through the chamber to establish a reference state (ref 1 in Scheme 1, i.e., the initial state). After establishing the reference line for incom-

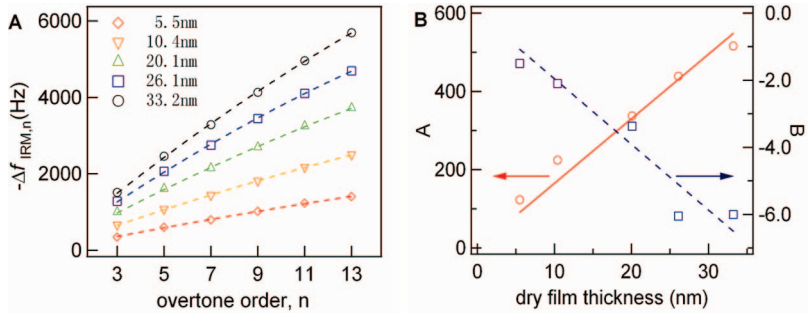

Figure 5. The frequency change dependence on overtone number *n*. (A) The value of Δf_{IRM} was plotted against *n* for different dry film thickness and fitted according to eq 8. (B) Fitted values of *A* and *B* show simple linear relations with dry film thickness (force to pass the original point), which was in agreement with eqs 9 and 10. The slope k_A was 16.5 ($R^2 \sim 0.95$) and k_B was −0.20 ($R^2 \sim 0.91$).

Table 3. Shear Compliance of Poly(OEGMA475) Brushes with Various Initiator Density and Thickness in Water Calculated from Equation 14

initiator density: 0.15		initiator density: 0.42		initiator density: 1.00	
T (nm)	J_f' (MPa^{-1})	T (nm)	J_f' (MPa^{-1})	T (nm)	J_f' (MPa^{-1})
4.1	$9.18n^{-0.68}$	6.2	$10.21n^{-0.67}$	7.7	$4.05n^{-0.39}$
7.7	$7.57n^{-058}$	8.7	$8.24n^{-0.61}$	11.3	$7.07n^{-0.72}$
11.4	$7.06n^{-0.66}$	10.9	$7.98n^{-0.67}$	15.0	$5.39n^{-0.58}$
19.2	$6.95n^{-0.61}$	11.8	$8.63n^{-0.64}$	18.5	$8.16n^{-0.71}$
21.6	$7.33n^{-0.56}$	18.6	$5.12n^{-0.40}$	20.0	$5.46n^{-0.58}$
		20.1	$8.05n^{-0.66}$	24.0	$4.25n^{-0.36}$

plete reaction mixture (IRM, ref 2 in Scheme 1), the complete reaction mixture (CRM) was introduced to the chamber and polymerization was initiated instantaneously. The polymerization was quenched when IRM and water were sequentially introduced to replace CRM, which resulted in the final reference lines (i.e., the final states). The values of Δf and ΔD were calculated to be the difference between the final state and initial state, i.e., the blue line and red line indicated Δf_{water} (polymer in water) and Δf_{IRM} (polymer in IRM), respectively. Note that we did not study the time evolution behavior (i.e., dynamics and kinetics), which will be reported elsewhere.

Figure 2 presented typical real time evolution of the $f-t$ curve (in blue) and the $D-t$ curve (in red) for the polymerization of OEGMA526. In the present experiment, the IRM was a mixture of methanol/water (50/50, v/v). The main reason why we tested multiple liquids is to see how the values of Δf and ΔD of poly(OEGMA526) brushes respond to the solvent changes. A previous report only looked at bare quartz crystal in water as the reference.[14]

In Figure 3A, the Δf_{water} of poly(OEGMA526) brushes was plotted with various film thicknesses against overtone number *n*. In this case, the bare quartz crystal in water was taken as the reference state and the quartz crystal with polymer brushes in water was the final state (i.e., ref 3). These data fitted well according to eq 8 (solid lines in Figure 3A), which resulted in *A* and *B*. In Figure 3B, the fitted parameters *A* and *B* were plotted against the dry film thickness ($t_{f,dry}$). There are two reasons for using $t_{f,dry}$ instead of wet film thickness, $t_{f,wet}$ (i.e., d_f in eqs 9 and 10): (1) we previously identified a constant swell ratio ($t_{f,wet}/t_{f,dry} = 2$) for poly(OEGMA),[21] (2) the measurement of $t_{f,dry}$ by ellipsometry in the air-solid mode is much easier than that of $t_{f,wet}$ in the liquid cell mode. Two linear relations, namely, $A-t_{f,dry}$ and $B-t_{f,dry}$, were identified, which was in agreement with eqs 9 and 10. Thus, we can calculate the density ρ_f and the shear compliance J_f'' of Poly(OEGMA526) brushes from the slopes (Figure 3B) according to eqs 15 and 16 and derived from eqs 9 and 10:

$$\rho_f = \frac{Z_q k_A}{4 f_0^2} \tag{15}$$

$$J_f'' = \frac{-Z_q k_B}{8\pi f_0^2 \rho_{liq} \eta_{liq}} \tag{16}$$

Note that $d_f = t_{f,wet} = 2t_{f,dry}$, leading to the algebraic numbers of $^1/_4$ and $^1/_8$ for eqs 15 and 16. Inserting these values $\rho_{water} = 1000$ kg m^{-3}, $\rho_{IRM} = 916$ kg m^{-3}, and $\eta_{water} = 0.89 \times 10^{-3}$ Pa s into eqs 15 and 16, the density of wet poly(OEGMA526) brushes was $\sim\rho_{f,wet} = 1521$ kg m^{-3}, while the shear compliance J_f'' was $\sim 0.57 \times 10^{-6}$ Pa^{-1} (Table 1).

The density of wet poly(OEGMA526) brushes obtained here (Table 1) was much smaller than those calculated (see Supporting Information) according to a previous published method based on the Voigt model.[27] Generally, the density of the polymeric material is around 1000 kg cm^{-3}. For examples, the densities of poly(ethylene glycol) (PEG) and poly(methyl methacrylate) (PMMA) are ~1120 and 1170 kg m^{-3}, respectively (http://www.sigma-aldrich.com). Thus, the value of $\rho_{f,wet}$ at 1521 kg m^{-3} was more reasonable for the wet poly(OEGMA526) brushes. On the other hand, the density of wet poly(OEGMA526) brushes can also be estimated at $\sim(1179 + 1000)/2 = 1089$ kg m^{-3} from the density $\rho_{f,dry}$ and the swelling ratio *R* of dry poly(OEGMA) brushes.[27]

(30) Hook, F.; Rodahl, M.; Kasemo, B.; Brzezinski, P. *Proc. Natl. Acad. Sci. U.S.A.* **1998**, *95*, 12271–12276.
(31) Keller, C. A.; Glasmastar, K.; Zhdanov, V. P.; Kasemo, B. *Phys. Rev. Lett.* **2000**, *84*, 5443–5446.
(32) Hook, F.; Kasemo, B.; Nylander, T.; Fant, C.; Sott, K.; Elwing, H. *Anal. Chem.* **2001**, *73*, 5796–5804.
(33) Zhang, G. Z. *Macromolecules* **2004**, *37*, 6553–6557.
(34) Liu, G. M.; Zhang, G. Z. *Langmuir* **2005**, *21*, 2086–2090.
(35) Liu, G. M.; Yan, S. H.; Zhang, G. Z. *J. Phys. Chem. B* **2007**, *111*, 3633–3639.
(36) Chen, H.; Su, X.; Neoh, K. G.; Choe, W. S. *Anal. Chem.* **2006**, *78*, 4872–4879.
(37) Su, X.; Lin, C. Y.; O'Shea, S. J.; Teh, H. F.; Peh, W. Y. X.; Thomsen, J. S. *Anal. Chem.* **2006**, *78*, 5552–5558.
(38) Hillman, A. R.; Efimov, I.; Skompska, M. *J. Am. Chem. Soc.* **2005**, *127*, 3817–3824.
(39) Ma, H. W.; Hyun, J. H.; Stiller, P.; Chilkoti, A. *Adv. Mater.* **2004**, *16*, 338–341.

The penetration depth δ of the shear wave in the liquid is given as

$$\delta = \sqrt{\frac{2\eta_l}{\omega\rho_l}} \tag{17}$$

where η_l and ρ_l are the viscosity and density of the liquid, respectively. For the frequency range used in the present experiments, the penetration depth δ of the shear wave in water ranged from 66 (65 MHz) to 137 nm (15 MHz), which was larger than the wet thickness of the polymer brushes. This suggests that the acoustic wave can still sense the whole film even at highest operating frequency of 65 MHz. Therefore, the physical parameters deduced from eqs 7−16 present the average properties of the polymer brushes.

In order to compare with the results obtained from the Voigt model, the shear compliance J_f'' can be used to estimate the viscosity η_f of the wet poly(OEGMA526) brushes via the relation of $J_f'' = (2\pi n f_0 \eta_f)^{-1}$. The viscosity η_f of the wet poly(OEGMA526) brushes was then $\sim 4.3 \times 10^{-3}$ to $\sim 19 \times 10^{-3}$ N s m^{-2} for the overtone $n = 3\sim13$, which was in the same order of magnitude as those obtained by the Voigt model. However, the frequency dependency of η_f was different. The Voigt model suggested a slight dependence of η_f on the overtone number n. While the direct application of eq 8 implied that J_f'' was independent of the frequency, leading to the n^{-1} dependence of η_f.

Similarly, ΔD_n was plotted against n (Figure 4A). However, one cannot use eq 13 to directly fit ΔD_n against n. The data suggests that the shear compliance J_f' may depend on the overtone number n (i.e., depend on the measuring frequency). Therefore, we applied eq 13 or eq 14 to calculate J_f' and plotted it against n (Figure 4B). (Note that eq 13 and eq 14 gave close results.) By assuming $G_f' \approx J_f'^{-1}$, the shear modulus of the poly(OEGMA526) brushes was estimated to be $\sim 10^5$ Pa (Table 2), which was in the same order of magnitude as those deduced from the Voigt model.[27] The shear modulus obtained here was found to scale as $G_f' \sim n^{0.6-1.0}$, which is also close to the results by the Voigt model. Interestingly, many groups already applied the plot of ΔD against Δf to indicate the physical state change although no clear meaning was given.[30−38]

The Voigt model predicts that a viscoelastic solid with one relaxation time has the frequency-dependent shear modulus and dynamic viscosity. At high frequency, G_f' scales as ω^2 and G_f'' is linear with ω. While the Maxwell model predicts that G_f' is independent of ω and G_f'' scales with ω^{-1} at high frequency for a viscoleastic fluid with one relaxation time. The relaxation time can be given as

$$\tau_f = \frac{\eta_f}{G_f'} \approx \frac{J_f'}{\omega J_f''} \tag{18}$$

From the above discussions, $\eta_f \sim n^{-1}$ and $G_f' \sim n^{0.6-1.0}$, leading to a distribution of relaxation time in the range of frequency studied. For example, the relaxation time was about 3.88×10^{-8} s for 20.1 nm thick poly(OEGMA526) brushes in water at the third overtone ($n = 3$). The experimental results indicate that the viscoelastic behavior of thin polymer brushes in liquid is complicated and can not be well predicted by the Voigt model or Maxwell model.

Wittmer et al. found that the relaxation time of an unentangled polymer brush in a good solvent can be estimated by[40]

$$\tau \cong \frac{\eta_l L^3}{k_{Boltz} T} \tag{19}$$

where $k_{Boltz} = 1.38 \times 10^{-23}$ J K^{-1} is the Boltzmann constant, T is absolute temperature, L is the length of brush, and η_l is the solvent viscosity. For the 20.1 nm thick poly(OEGMA526) brush in water, the length L was assumed to be $t_{f,wet}$, i.e., $\sim$ 40.2 nm. The relaxation time was then estimated from eq 19 to be 1.4×10^{-5} s at 25 °C, which is about 3 orders of magnitude larger than those from eq 18. This result suggests that the dynamic of polymer brushes is much faster at high frequency. Equation 19 may pertain to the longest relaxation time, which is very long because of the chain attachment to the surface. The QCM cannot probe such a long relaxation mode since it is operated at high frequency. However, there are many other fast modes of segmental relaxation, which soften the polymer and can be assessed by QCM. Furthermore, eq 19 predicts that the relaxation time increases with increasing the length of polymer brushes and the solvent viscosity. Interestingly, the shear modulus of poly(OEGMA526) brushes was found to be only slightly dependent on the film thickness, and η_f was independent of the film thickness in the experimental range. The relaxation time of poly(OEGMA526) brushes hence was only slightly dependent on the film thickness. No systematic behavior was observed. On the other hand, the relaxation time of poly(OEGMA526) brushes was also only slightly dependent on the solvent viscosity (i.e., the viscosity difference between water and the mixture of water and methanol (IRM), see below for details).

We then continued to study the behavior of poly(OEGMA526) brushes in IRM, where the bare quartz crystal in IRM was taken as the reference state and the quartz crystal with polymer brushes in IRM was the final state (i.e., ref 2). The results were listed in Table 1. Clearly, eq 8 fitted well to the experimental data as well (dashed lines in Figure 5A). In this case, the density of wet poly(OEGMA526) brushes was obtained to be $\sim \rho_{f,wet} = 1452$ kg m^3, while the shear compliance J_f'' was ~ 0.64 MPa^{-1}. Note that $\eta_{IRM} = 1.76 \times 10^{-3}$ Pa s was measured by QCM-D according to ref 22. J_f' was similar to those obtained in water (Table 2). The results obtained by taking the bare quartz crystal in the IRM mixture as the reference state were similar to those when using the bare quartz crystal in pure water as the reference state, indicating poly(OEGMA526) had a minimal response to water and IRM exchange. Again, a distribution of relaxation times was found for poly(OEGMA526) brushes in IRM. The relaxation time was about 3.49×10^{-8} s for 20.1 nm thick poly(OEGMA526) brushes in IRM at the third overtone ($n = 3$), which was slightly smaller than that in water.

We further applied eqs 8 and 14 to analyze the published data on monomer OEGMA475; the detailed calculation can be found in the Supporting Information and listed in Tables 1 and 3. It was expected that the shear modulus of poly(OEGMA475) and

(40) Wittmer, J.; Johner, A.; Joanny, J. F. *Colloids Surf., A* **1994**, *86*, 85–89.

poly(OEGMA526) shared a similar value and trend of dependence on overtone number n ($\sim 5n^{-0.6}$ MPa^{-1}) because these two monomers were similar in molecular weight and only different in the terminal group, OEGMA475 was terminated with a $-CH_3$ group and OEGMA526 was terminated with a $-OH$ group (see Supporting Information).

CONCLUSION

In conclusion, we demonstrated that by converting D to Γ, the equations based on Δf and $\Delta\Gamma$ (eqs 8, 13, and 14) can be applied to interpret the data of QCM-D. The viscoelastic parameters obtained were in the same order of magnitude as those from the Voigt model although the frequency dependence was slightly different. In another way, the Voigt model can be used to analyze the data obtained from network analysis. Thus, a general method may be deduced for the analyses of QCM data. One advantage of the herein presented equation is that it can analyze a single data point while the Voigt model method requires at least three points of different film thickness,[22] which was a formidable challenge for most biological samples.

QCM has achieved great success in recent years, partially due to its direct visualization of dissipation, easy of use, its ability to be coupled with other techniques,[41,42] and quick data-acquisition rate, which is strongly needed for the real time kinetic measurements such as in the field of biosensor applications[43] and fundamental studies.[44] We believe that the incorporation of SI-ATRP technology in QCM studies will greatly promote the development of these fields in that (i) the in situ film deposition method minimizes error caused by the loading and unloading operations,[27] (ii) SI-ATRP provides a fine control over film thickness and density that gives a diverse sample pool for QCM studies that probes the dynamic of polymer brush in liquid at high frequency, and (iii) SI-ATRP synthesizes the functional matrix for biosensor applications.[45]

(41) Wang, Z. H.; Kuckling, D.; Johannsmann, D. *Soft Mater.* **2003**, *1*, 353–364.
(42) Plunkett, M. A.; Wang, Z. H.; Rutland, M. W.; Johannsmann, D. *Langmuir* **2003**, *19*, 6837–6844.
(43) Ward, M. D.; Buttry, D. A. *Science* **1990**, *249*, 1000–1007.
(44) Fytas, G.; Anastasiadis, S. H.; Seghrouchni, R.; Vlassopoulos, D.; Li, J. B.; Factor, B.; Theobald, W.; Toprakcioglu, C. *Science* **1996**, *274*, 2041–2044.
(45) Tsujii, Y.; Ohno, K.; Yamamoto, S.; Goto, A.; Fukuda, T. *Adv. Polym. Sci.* **2006**, *197*, 1–45.

ACKNOWLEDGMENT

We thank L. Fu and J. A. He for assistance in the SIP experiments. This project was supported by the NSFC Grant 20604002 and NSFB Grant 2072008 to H. Ma and by NSFC Grant 20604022, Scientific Research Foundation for Returned Overseas Chinese Scholars (Ministry of Education), and the Zhejiang Provincial Natural Science Foundation of China (Grant Y406029) to B. Du.

SUPPORTING INFORMATION AVAILABLE

Additional information as noted in text. This material is available free of charge via the Internet at http://pubs.acs.org.

Received for review September 18, 2008. Accepted November 20, 2008.

AC8019762